Nonparaxial propagation properties of an anomalous hollow beam with orbital angular momentum

Zhu, Xinlei; Lu, Xingyuan; Wang, Kuilong; Zhao, Chengliang; Hoenders, Bernhard J.; Cai, Yangjian

Published in:
Journal of modern optics

DOI:
10.1080/09500340.2017.1330434

Publication date:
2017

Journal of Modern Optics

ISSN: 0950-0340 (Print) 1362-3044 (Online) Journal homepage: https://www.tandfonline.com/loi/tmop20

Nonparaxial propagation properties of an anomalous hollow beam with orbital angular momentum

Xinlei Zhu, Xingyuan Lu, Kuilong Wang, Chengliang Zhao, Bernhard J. Hoenders & Yangjian Cai

To cite this article: Xinlei Zhu, Xingyuan Lu, Kuilong Wang, Chengliang Zhao, Bernhard J. Hoenders & Yangjian Cai (2017) Nonparaxial propagation properties of an anomalous hollow beam with orbital angular momentum, Journal of Modern Optics, 64:19, 1960-1970, DOI: 10.1080/09500340.2017.1330434

To link to this article: https://doi.org/10.1080/09500340.2017.1330434

Published online: 26 May 2017.

JOURNAL OF MODERN OPTICS, 2017
VOL. 64, NO. 19, 1960–1970
https://doi.org/10.1080/09500340.2017.1330434

Taylor & Francis
Taylor & Francis Group

Nonparaxial propagation properties of an anomalous hollow beam with orbital angular momentum

Xinlei Zhu[a,b], Xingyuan Lu[a,b], Kuilong Wang[c], Chengliang Zhao[a,b], Bernhard J. Hoenders[d] and Yangjian Cai[a,b]

[a]College of Physics, Optoelectronics and Energy and Collaborative Innovation Center of Suzhou Nano Science and Technology, Soochow University, Suzhou, China; [b]Key Lab of Advanced Optical Manufacturing Technologies of Jiangsu Province and Key Lab of Modern Optical Technologies of Education Ministry of China, Soochow University, Suzhou, China; [c]Department of Physics, Hangzhou Normal University, Hangzhou, China; [d]Zernike Institute for Advanced Materials, University of Groningen, Groningen, The Netherlands

ABSTRACT

The analytical nonparaxial propagation formula of an anomalous hollow beam (AHB) with orbital angular momentum (OAM) in free space is derived based on the generalized Raleigh–Sommerfeld diffraction integral. The nonparaxial properties of AHB with OAM such as intensity, phase and OAM density distributions are studied in detail, using the pertinent nonparaxial propagation formula. The comparison between the paraxial and nonparaxial results is also carried out. The results show that the nonparaxial properties of an AHB with OAM are determined by the initial beam parameters, such as beam waist size and topological charge and propagation distance.

ARTICLE HISTORY
Received 6 April 2017
Accepted 6 May 2017

KEYWORDS
Orbital angular momentum; nonparaxial propagation; anomalous hollow beam

1. Introduction

A beam with spiral-type phase distribution is called a vortex beam. At the centre of a vortex beam the intensity distribution is zero. It has been shown in recent years that there are phase singularities in a vortex beam, and each photon of the vortex beam carries an orbital angular momentum (OAM). Due to many applications, such as particle capture and manipulation, optical information coding and transmission, atomic optics, optical tweezers, quantum information processing, as well as the autofocusing properties and the vectorial structure (*1–8*), the vortex beams have attracted more and more attention. Moreover, there are many experimental methods to produce vortex beams (*9–11*).

On the other hand, with the development of laser technology, it has become possible to generate all kinds of beams with zero intensity at the centre, thus creating a new so-called dark hollow beams (DHBs) family. Theoretical and experimental studies show that the DHBs have many applications in the fields of atomic optics, free-space optical communications, binary optics, optical trapping of particles and medical sciences (*12–15*). Various techniques have been used to generate DHBs, such as the computer-generated hologram, the transverse mode selection method, the geometrical optical method, spatial filtering, etc. (*16–20*).

Until now, many theoretical models have been proposed to describe DHBs, such as the Bessel–Gaussian beams, LG modes, hollow Gaussian beams, dark hollow beams, higher order Mathieu beams and so on (*21–25*). In 2005, Wu et al. demonstrated experimentally for the first time an anomalous hollow beam (AHB) of elliptical symmetry with an elliptical solid core. In 2007 and 2008, Cai proposed two convenient theoretical models to describe AHB (*9, 10*). The main difference between conventional DHB and AHB is that the central intensity of the conventional DHB is zero, while the central part of an AHB has an elliptical or circular solid core.

In Cai's theoretical models, the electric field of an AHB is expressed as a superposition of finite sums of astigmatic Gaussian modes and astigmatic doughnut modes. Since then, within the paraxial approximation, the propagation properties of coherent and partially coherent AHB under various cases have been widely studied (*26–31*). In 2014, Zhao introduced a new theoretical model to describe the AHB with OAM, and studied the effect of the topological charge (TC) on the propagation properties of the AHB with OAM numerically (*32*). From their results, one can

CONTACT Chengliang Zhao zhaochengliang@suda.edu.cn

find that the propagation properties of the AHB with OAM are completely different with the AHB. The AHB with OAM can keep dark hollow distribution in the far field. Therefore, the AHB with OAM can applied in the free-space optical communication.

As we know, the paraxial approximation is no longer valid when the far-field divergent angle becomes large or when the beam spot size and wavelength are comparable. To the best of our knowledge, no results have been published up until now on nonparaxial propagation of an AHB with OAM. However, the nonparaxial propagation conditions are always encountered in highly focused optical system such as objective with high numerical aperture and holography microscopy. Therefore, it's interesting to study the nonparaxial propagation of the AHB with OAM. In this paper, based on the Rayleigh–Sommerfeld integrals formula, an analytical expression of the nonparaxial AHB with OAM in free space is derived. The normalized intensity, phase, and the OAM density distribution of the nonparaxial AHB with OAM propagating in free space are numerically studied in detail.

2. Theory

The electric field of the general AHB with OAM in the source plane $z = 0$ takes the form (*32*):

$$E(x,y,0) = \left(-2 + \frac{8x^2}{w_{0x}^2} + \frac{8y^2}{w_{0y}^2}\right) \exp\left(-\frac{x^2}{w_{0x}^2} - \frac{y^2}{w_{0y}^2}\right) \times (x+iy)^M. \tag{1}$$

In the Cartesian coordinate system, consider an AHB with OAM linearly polarized in the x direction. The electric field can be rewritten as

$$\begin{pmatrix} E_x(x,y,0) \\ E_y(x,y,0) \end{pmatrix} = \begin{pmatrix} \left(-2 + \frac{8x^2}{w_{0x}^2} + \frac{8y^2}{w_{0y}^2}\right) \exp\left(-\frac{x^2}{w_{0x}^2} - \frac{y^2}{w_{0y}^2}\right)(x+iy)^M \\ 0 \end{pmatrix}, \tag{2}$$

where w_{0x} and w_{0y} are the beam waist width of an astigmatic Gaussian mode in x and y directions, respectively. M is TC and also denotes the number of 2π phase cycles around the optical vortex centred on the optical axial.

Based on the Rayleigh–Sommerfeld integral formula, the nonparaxial AHB propagating towards the free space $z > 0$ can be described as (*33*)

$$E_x(\boldsymbol{r}) = -\frac{1}{2\pi}\int_{-\infty}^{\infty}\int_{-\infty}^{\infty} E_x(x_0,y_0,0)\frac{\partial \boldsymbol{G}(\boldsymbol{r},\boldsymbol{r}_0)}{\partial z}\mathrm{d}x_0\mathrm{d}y_0, \tag{3}$$

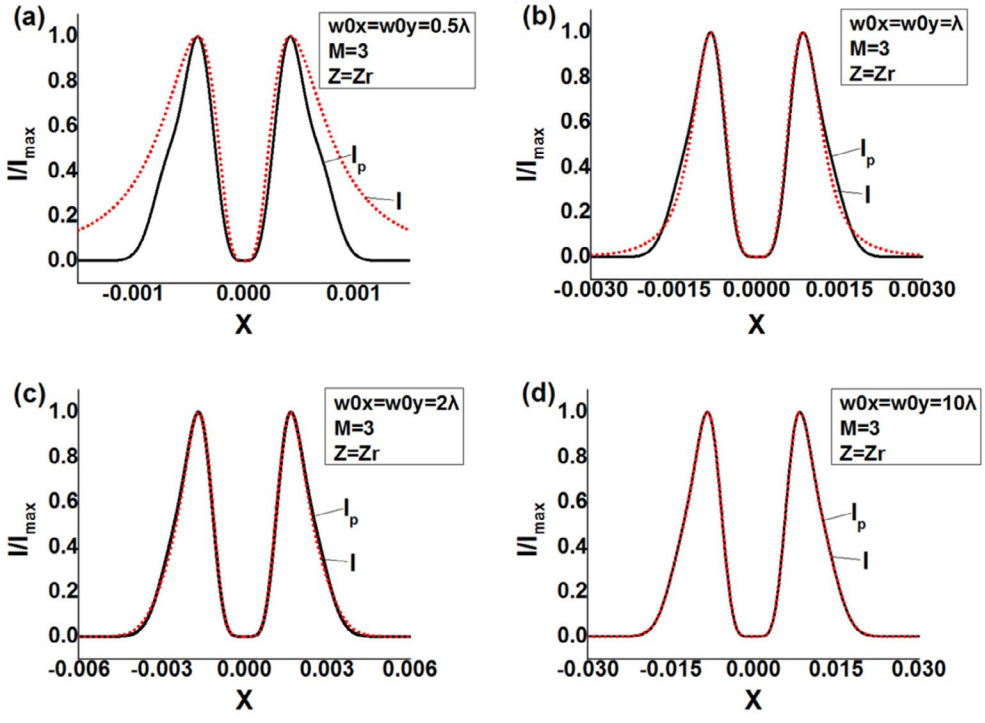

Figure 1. The normalized intensity of an AHB with OAM of circular symmetry in the free space with different beam waists: $z = z_r$, $M = 3$, where the solid and dotted curves denote the nonparaxial and paraxial results, respectively.

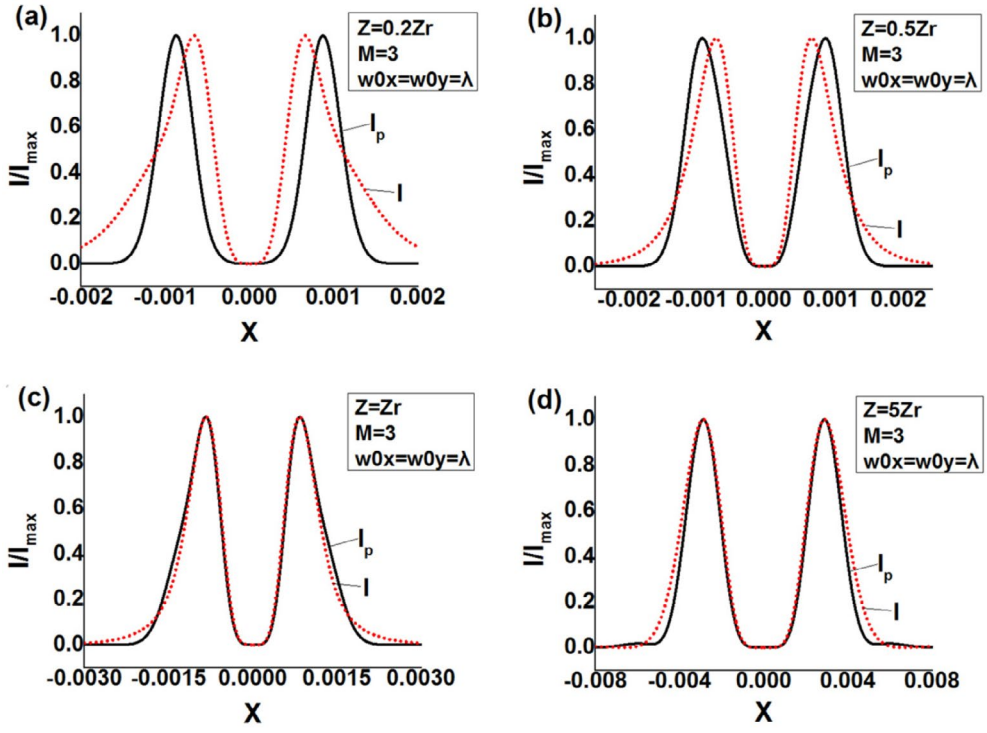

Figure 2. The normalized intensity of an AHB with OAM of circular symmetry in the free space with different propagation distances: $w_{0x} = w_{0y} = \lambda$, $M = 3$, where the solid and dotted curves denote the nonparaxial and paraxial results, respectively.

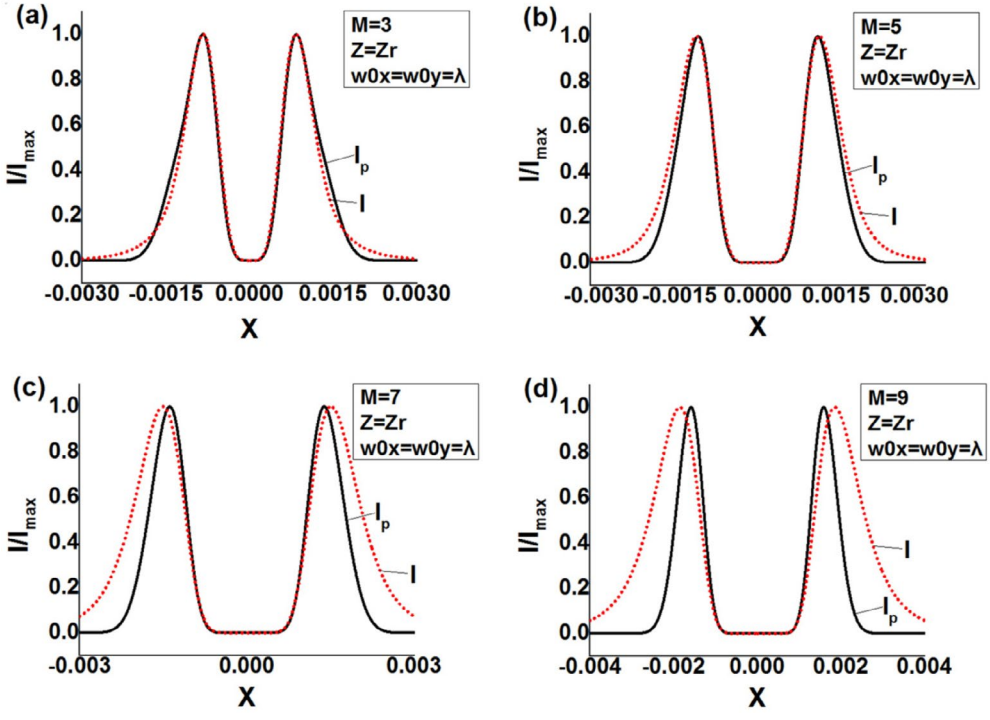

Figure 3. The normalized intensity of an AHB with OAM of circular symmetry in the free space with different TC: $w_{0x} = w_{0y} = \lambda$, $z = z_r$, where the solid and dotted curves denote the nonparaxial and paraxial results, respectively.

$$E_y(\boldsymbol{r}) = -\frac{1}{2\pi}\int_{-\infty}^{\infty}\int_{-\infty}^{\infty} E_y(x_0, y_0, 0)\frac{\partial \boldsymbol{G}(\boldsymbol{r}, \boldsymbol{r}_0)}{\partial z}\mathrm{d}x_0\mathrm{d}y_0, \quad (4)$$

$$E_z(\boldsymbol{r}) = \frac{1}{2\pi}\int_{-\infty}^{\infty}\int_{-\infty}^{\infty}\left[E_x(x_0, y_0, 0)\frac{\partial \boldsymbol{G}(\boldsymbol{r}, \boldsymbol{r}_0)}{\partial x} + E_y(x_0, y_0, 0)\frac{\partial \boldsymbol{G}(\boldsymbol{r}, \boldsymbol{r}_0)}{\partial y}\right]\mathrm{d}x_0\mathrm{d}y_0, \quad (5)$$

where

$$\boldsymbol{G}(\boldsymbol{r}, \boldsymbol{r}_0) = \frac{\exp\left(ik|\boldsymbol{r} - \boldsymbol{r}_0|\right)}{|\boldsymbol{r} - \boldsymbol{r}_0|}, \quad (6)$$

$r = x\boldsymbol{i} + y\boldsymbol{j} + z\boldsymbol{k}$ and $r_0 = x_0\boldsymbol{i} + y_0\boldsymbol{j}$ with $\boldsymbol{i}$,$\boldsymbol{j}$ and $\boldsymbol{k}$ being units of vectors of x-, y- and z-axes in the Cartesian coordinate system, respectively, and $k = 2\pi/\lambda$ is the wave number with λ being the incident wavelength.

In the nonparaxial approximation of the near field, we have the following approximation:

$$\boldsymbol{G}(\boldsymbol{r}, \boldsymbol{r}_0) = \frac{1}{r}\exp\left[ik\left(r + \frac{x_0^2 + y_0^2 - 2xx_0 - 2yy_0}{2r}\right)\right], \quad (7)$$

where $r = \left(x^2 + y^2 + z^2\right)^{1/2}$.

In the case of far field sources, Equation (7) can be further simplified into the following form:

$$\boldsymbol{G}(\boldsymbol{r}, \boldsymbol{r}_0) = \frac{1}{r}\exp\left[ik\left(r + \frac{-2xx_0 - 2yy_0}{2r}\right)\right]. \quad (8)$$

Substituting Equations (2) and (7) into Equations (3)–(5), using the following expansion and mathematical integral formula:

$$\left(x + iy\right)^M = \sum_{l=0}^{M}\frac{M!i^l}{l!(M-l)!}, \quad (9)$$

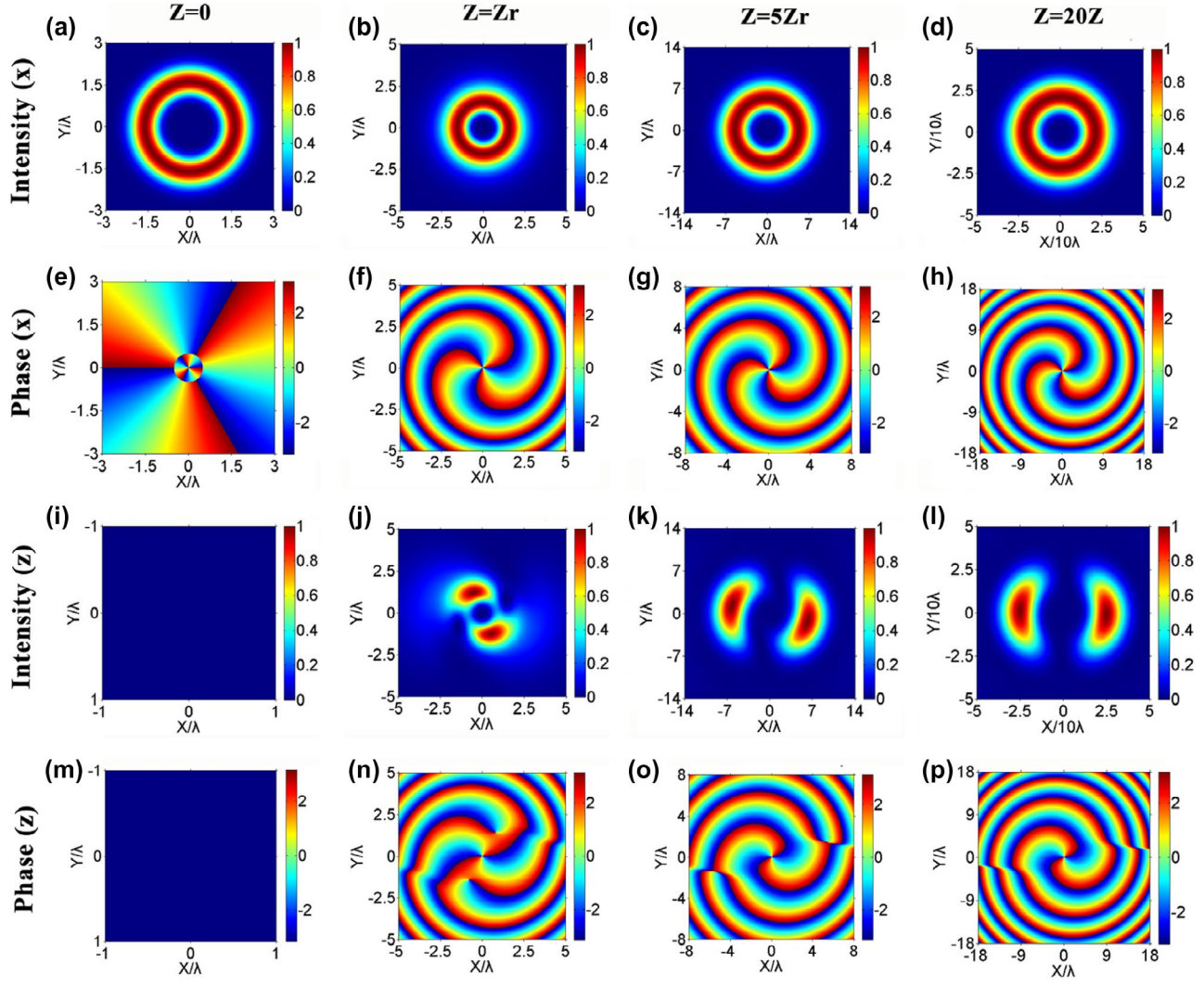

Figure 4. The normalized intensity and the phase distributions of the nonparaxial AHB with OAM of circular symmetry in the free space for different propagation distances: $w_{0x} = w_{0y} = \lambda$, $M = 3$.

$$\int_{-\infty}^{\infty} x^n e^{-px^2+2qx}\mathrm{d}x = n!e^{q^2/p}\sqrt{\frac{\pi}{p}}\left(\frac{q}{p}\right)^n \sum_{k=0}^{[n/2]} \frac{1}{(n-2k)!(k)!}\left(\frac{p}{4q^2}\right)^k. \tag{10}$$

A tedious, but straightforward integration, leads to the following expression for an AHB with OAM in the non-paraxial approximation:

$$E_x(r) = -\frac{ikz}{2\pi r^2}\sum_{l=0}^{M}\frac{M!i^l}{l!(M-l)!}\exp(ikr) \times \left[\left(-2N_{10}+\frac{8}{w_{0x}^2}N_{12}\right)N_{20}+\frac{8}{w_{0y}^2}N_{10}N_{22}\right], \tag{11}$$

$$E_y(r) = 0, \tag{12}$$

$$E_z(r) = -\frac{ikz}{2\pi r^2}\sum_{l=0}^{M}\frac{M!i^l}{l!(M-l)!}\exp(ikr) \times \left[\left(-2xN_{10}+2N_{11}+\frac{8x}{w_{0x}^2}N_{12}-\frac{8}{w_{0x}^2}N_{13}\right)N_{20} + \left(\frac{8x}{w_{0y}^2}N_{10}-\frac{8}{w_{0y}^2}N_{11}\right)N_{22}\right], \tag{13}$$

where

$$N_{ij} = n_{ij}!e^{q_x^2/p_x}\sqrt{\frac{\pi}{p_x}}\left(\frac{q_x}{p_x}\right)^{n_{ij}}\sum_{k=0}^{[n_{ij}/2]}\frac{1}{\left(n_{ij}-2k\right)!(k)!}\left(\frac{p_x}{4q_x^2}\right)^k, \tag{14}$$

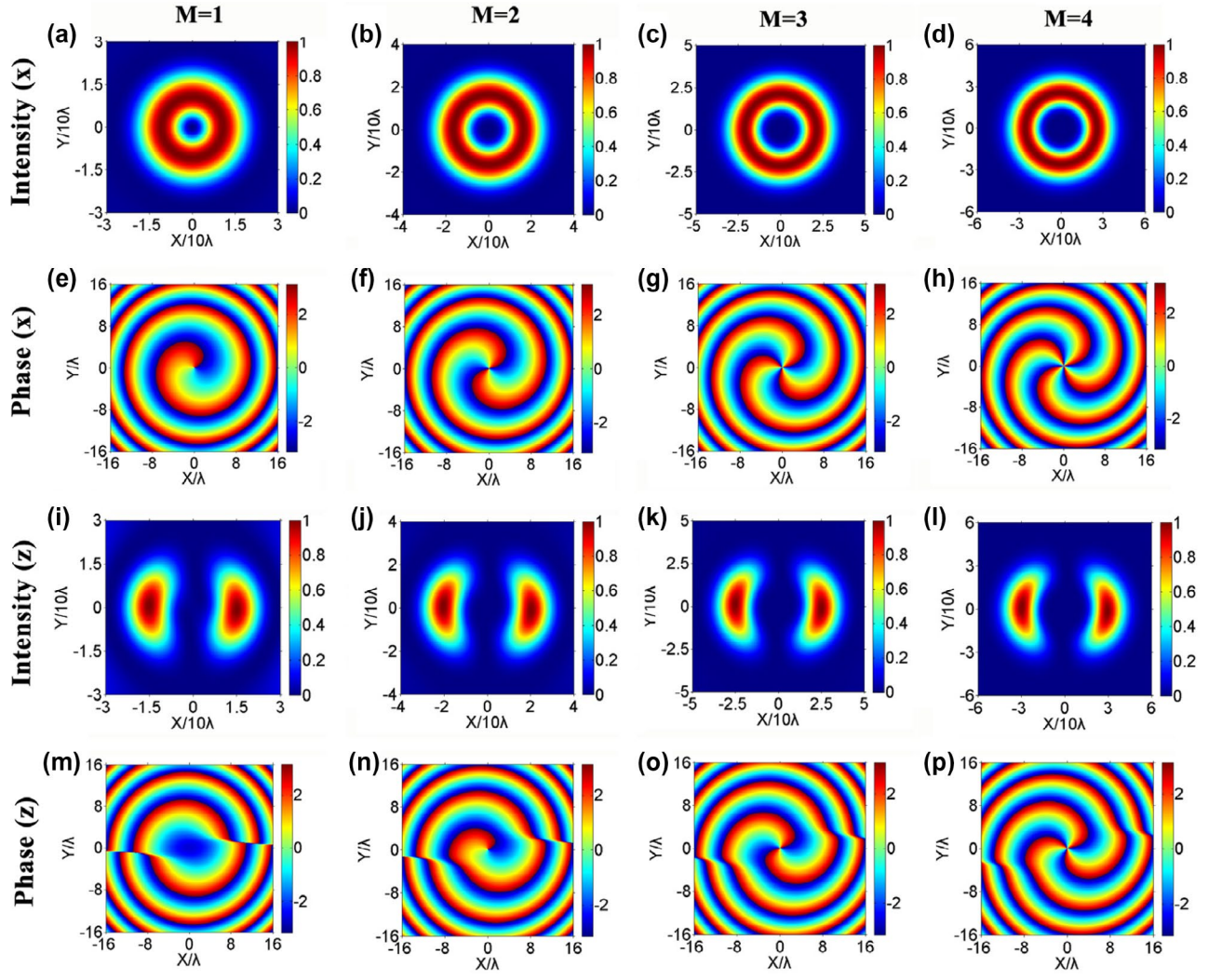

Figure 5. The normalized intensity and the phase distributions of the nonparaxial AHB with OAM of circular symmetry in the free space for different TC: $w_{0x} = w_{0y} = \lambda$, $z = 20z_r$.

$$p_x = \frac{1}{w_{0x}^2} - \frac{ik}{2r},\ p_y = \frac{1}{w_{0y}^2} - \frac{ik}{2r},\ q_x = -\frac{ikx}{2r},\ q_y = -\frac{iky}{2r}, \tag{15}$$

$$n_{10} = M - l,\ n_{11} = M - l + 1,\ n_{12} = M - l + 2,\ n_{13} = M - l + 3, \tag{16}$$

$$n_{20} = l,\ n_{22} = l + 2. \tag{17}$$

Then substituting Equations (2) and (8) into Equation (3–5), we obtain the following far-field expression for the nonparaxial AHB with OAM:

$$E_x(r) = -\frac{ikz}{2\pi r^2}\sum_{l=0}^{M}\frac{M!i^l}{l!(M-l)!}\exp(ikr) \times \left[\left(-2H_{10} + \frac{8}{w_{0x}^2}H_{12}\right)H_{20} + \frac{8}{w_{0y}^2}H_{10}H_{22}\right] \tag{18}$$

$$E_y(r) = 0 \tag{19}$$

$$E_z(r) = -\frac{ikz}{2\pi r^2}\sum_{l=0}^{M}\frac{M!i^l}{l!(M-l)!}\exp(ikr) \times \left[\left(-2xH_{10} + 2H_{11} + \frac{8x}{w_{0x}^2}H_{12} - \frac{8}{w_{0x}^2}H_{13}\right)H_{20} + \left(\frac{8x}{w_{0y}^2}H_{10} - \frac{8}{w_{0y}^2}H_{11}\right)H_{22}\right], \tag{20}$$

where $H_{ij} = n_{ij}!e^{k_x^2/g_x}\sqrt{\frac{\pi}{g_x}}\left(\frac{k_x}{g_x}\right)^{n_{ij}}\sum_{k=0}^{\left[n_{ij}/2\right]}\frac{1}{(n_{ij}-2k)!(k)!}\left(\frac{k_x}{4g_x^2}\right)^k$, $g_x = \frac{1}{w_{0x}^2}$, $g_y = \frac{1}{w_{0y}^2}$, $k_x = -\frac{ikx}{2r}$, $k_y = -\frac{iky}{2r}$, other expression of n_{10}, n_{11}, n_{12}, n_{13}, $n_{20}$and n_{22} are same as Equations (16) and (17).

The propagation expression of the AHB with OAM in the paraxial regime can be treated as a special case by using the paraxial expansion

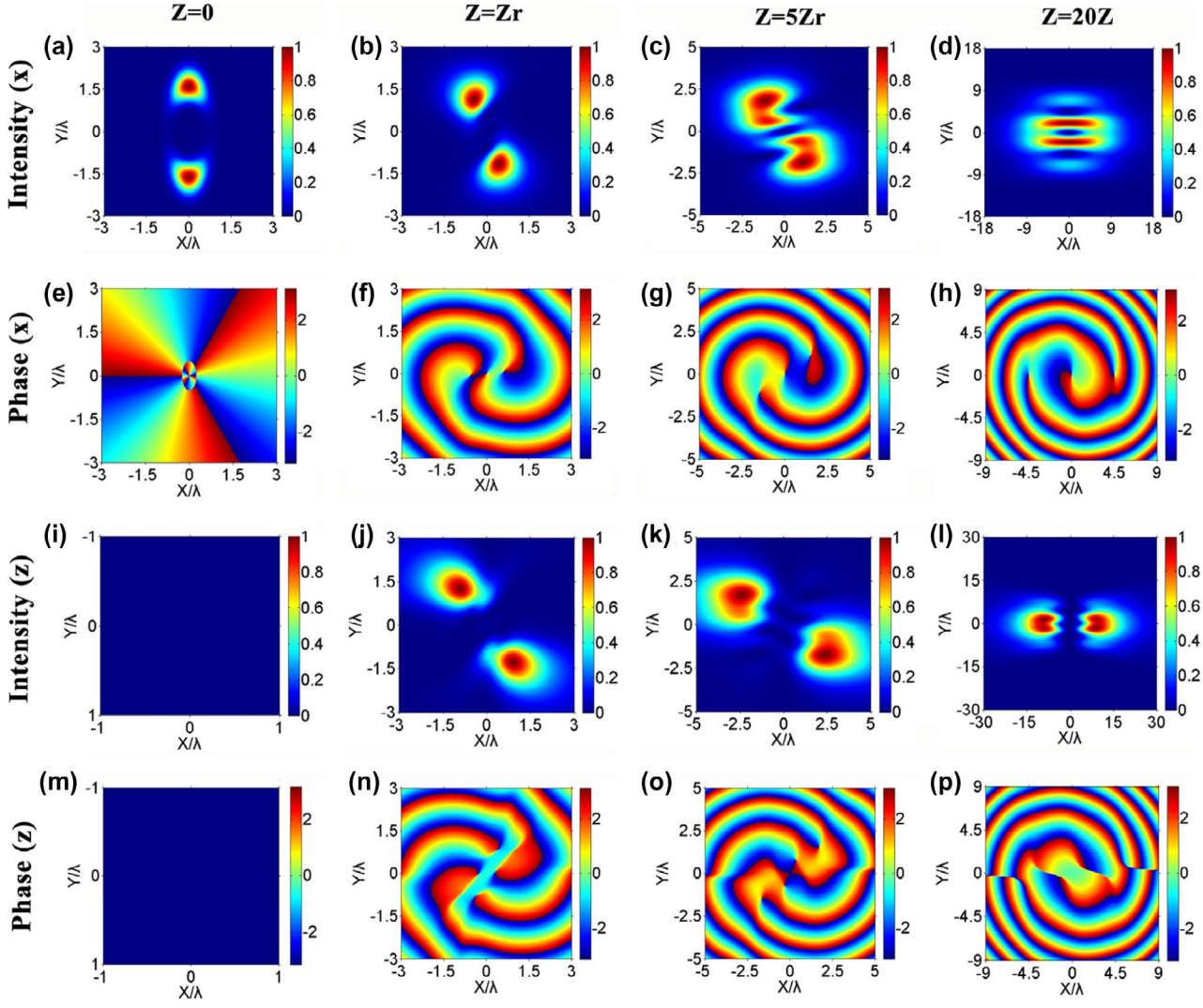

Figure 6. The normalized intensity and the phase distributions of the nonparaxial AHB with OAM of elliptical symmetry in the free space for different propagation distances: $w_{0x} = 0.5\,\lambda$ $w_{0y} = \lambda$, $M = 3$.

$$r \approx z + \frac{x^2 + y^2}{2z}. \tag{21}$$

Replacing r of the exponential part in Equations (11–13) and other terms with z, we obtain the propagation expression of AHB with OAM passing through the paraxial free-space.

Each photon of the vortex beam carries an OAM of $M\hbar$, where $\hbar$ is the reduced Planck constant. The orbital angular momentum density distribution of an AHB with OAM is given by

$$J_z = \frac{i\varepsilon_0}{\omega}\left\{x\left[E^*\frac{\partial E}{\partial y} - E\frac{\partial E^*}{\partial y}\right] - y\left[E^*\frac{\partial E}{\partial x} - E\frac{\partial E^*}{\partial x}\right]\right\}. \tag{22}$$

where ω is the circular frequency, and ε_0 is the electric permittivity of vacuum. E is the abbreviation of $E_x(r)$.

3. Numerical calculations and analyses

Based on the propagation formulae Equations (11–13), obtained in Section 2, we can study the nonparaxial propagation properties of an AHB with OAM in free space. The optical wavelength is set to be $\lambda = 532$ nm. The light intensity is given by $I = |E_x|^2 + |E_y|^2 + |E_x|^2$.

Figures 1–3 show the normalized intensity of an AHB with OAM in the free space with different beam waist w, propagation distance z and topological charge M. The solid curves denote the nonparaxial results obtained by using Equations (11–13) and (18–20), and the dotted curves denote the paraxial results obtained by using Equations (11–13) and (22). Here, $z_r = kw_{0x}^2/2$ is the confocal parameter of the Gaussian part. The corresponding paraxial results are also calculated for the convenience of comparison. From Figure 1, we can see that, with increasing width of the beam waist, the difference between the

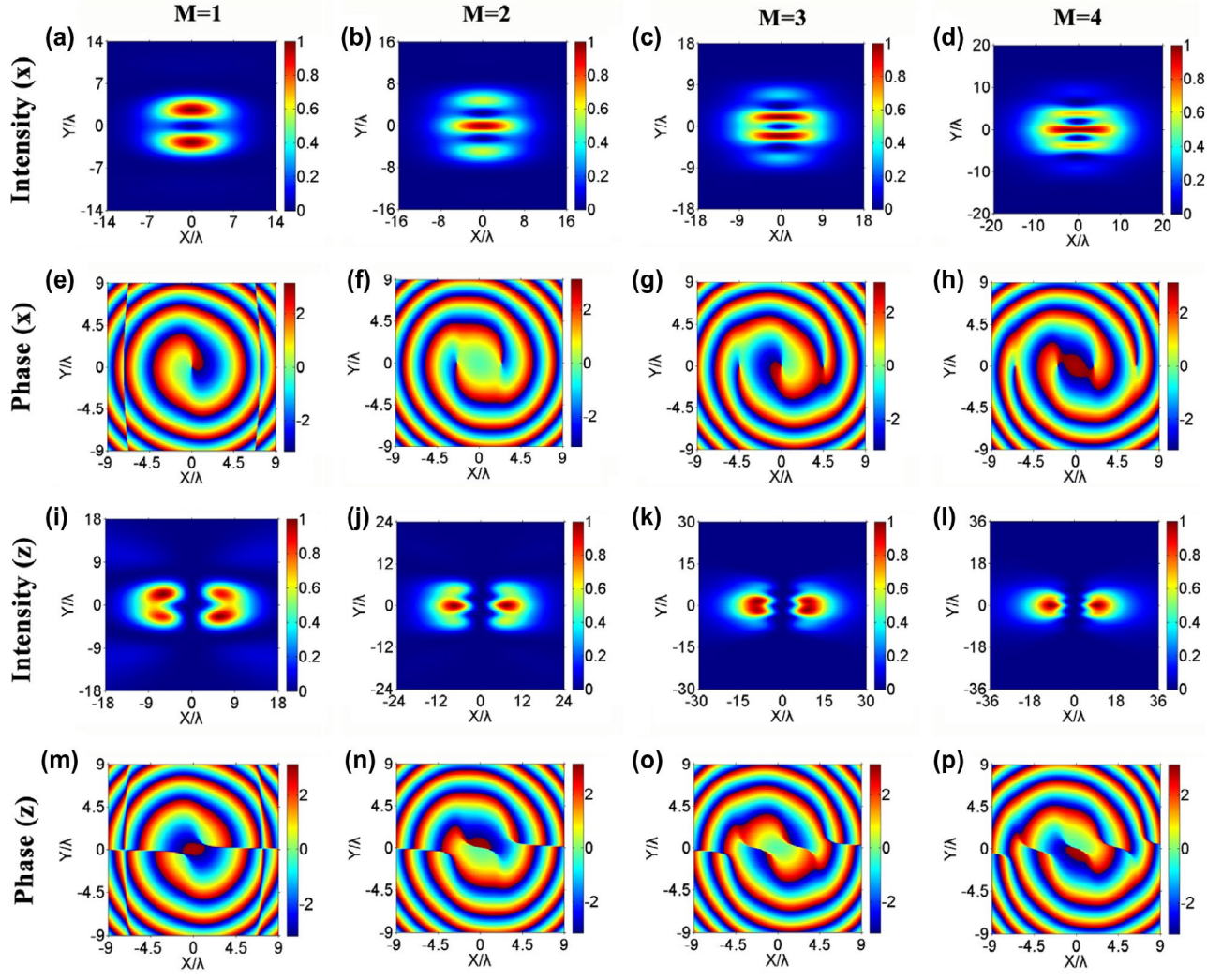

Figure 7. The normalized intensity and the phase distributions of the nonparaxial AHB with OAM of elliptical symmetry in the free space for different TC: $w_{0x} = 0.5 = \lambda$, $w_{0y} = \lambda$, $z = 20z_r$.

normalized light intensities arising from nonparaxial to paraxial propagation decreases gradually (Figure 1(a) and (b)). When the initial beam waist $w_{0x} = w_{0y}$ is much larger than λ, the difference between the nonparaxial and paraxial results can be neglected (Figure 1(d)). This means that the paraxial approximation is valid also in the nonparaxial case. From Figure 2, one can find that the difference between the nonparaxial and paraxial is obviously large in the near field (Figure 2(a)) if $w_{0x} = w_{0y} = \lambda$, while it disappears in the far field (Figure 2(d)). From Figure 3, we can find that the influence of topological charge M on the propagation properties of the AHB with OAM is significant, and the difference between the nonparaxial and paraxial results becomes evident as the topological charge decreases.

To learn more about the influences of the initial beam parameters and propagation distance on the evolution properties of the nonparaxial AHB with OAM in free space, we carried out the calculations for different values of the pertinent parameters (propagation distance, initial beam parameters). Figures 4–7 show the contour graphs of the normalized intensity and phase distributions of the nonparaxial AHB with OAM of circular symmetry and elliptical symmetry in free space for different values of the propagation distance z, the M, and the initial beam waists. The first and second rows in Figures 4–7 are the intensity and phase distributions of x-component, and the third and fourth row are intensity and phase distributions of z-component. From the first row of Figures 4 and 5, we can find that the evolution, of the intensity distribution of the x-component of the nonparaxial AHB with OAM for different M and z is very stable. The beam profile keeps the dark hollow distribution for different values of z and M. The second row of Figures 4 and 5 shows the corresponding phase distribution. The curves of equiphase become heliciform and counterclockwise for positive values of M, and the numbers of petals is equal to the absolute value of M. From the third row of Figures 4 and 5, we can see that the intensity distribution of the z-component of a nonparaxial AHB with AOM is different from the intensity distribution of the x-component (see first row Figures 4 and 5): this distribution is zero in the source

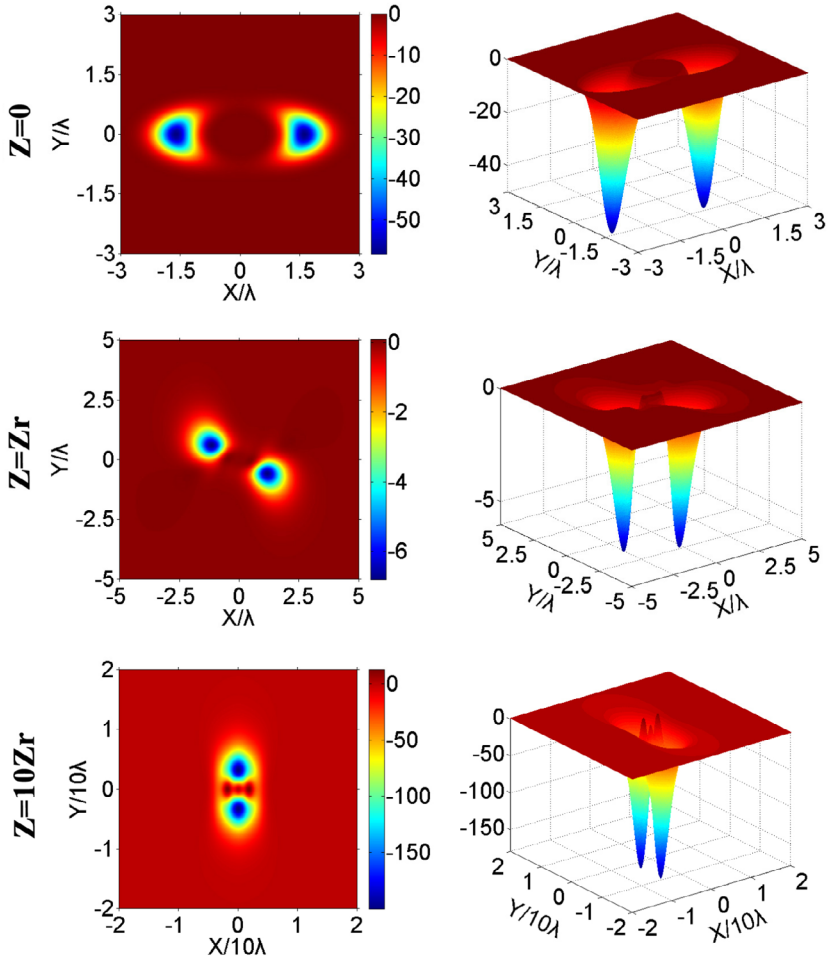

Figure 8. The OAM density distribution of the nonparaxial AHB with OAM of elliptical symmetry in the free space for different propagation distances: $w_{0x} = 0.5\,\lambda$, $w_{0y} = \lambda$, $M = 3$.

plane, but is no longer equal to zero upon propagation. This is due to a change of the polarization state of the radiation. Numerical results (not given in here) show that the intensity of the z-component in the nonparaxial regime is much smaller than that of the x-component. As the propagation distance z increases, the beam profile of the z-component changes gradually from one distorted lobe to two lobes, distributed in x-direction. The phase distribution of the z-component of the nonparaxial AHB with AOM is also different from that of the x-component (see second row Figures 4 and 5). A lateral dislocation appears, and the direction of transverse dislocation changes with the propagation distance.

Figures 6 and 7 show the contour graphs of the normalized intensity and phase distributions of the nonparaxial AHB with OAM with elliptical symmetry. In Figure 6, $w_{0x} = 0.5\lambda$, $w_{0y} = \lambda$, $M = 3$, the other parameters are same as Figures 4 and 5. From Figure 6, one can find that the intensity distribution of the nonparaxial AHB with OAM with elliptical symmetry is different from those with circular symmetry (see Figure 4). With the increase of the propagation distance, the intensity distribution in the x-direction expands faster than that in the y-direction (see Figure 6(a)–(d)). The behaviour in case of an AHB with elliptic symmetry and OAM is similar to an AHB with OAM with circular symmetry: Though the z-component is zero in the source plane (see Figure 6(i)), its intensity becomes non-zero with increasing propagation distance. The spot profile also experiences a rotation and finally takes on a transverse symmetric distribution. From the second and the fourth row in Figure 6, one can see that the phase distributions of the x-component of a non-paraxial AHB with elliptical symmetry and with OAM are radial lines in the source plane. In the central region, there is another elliptic region containing equiphase curves which are also radial lines. With the increase of the propagation distance, the phase distributions of the x-component and z-component are also heliciforms, but the helix is not smooth, there is a certain distortion. In the central region, the distortion increases with increasing

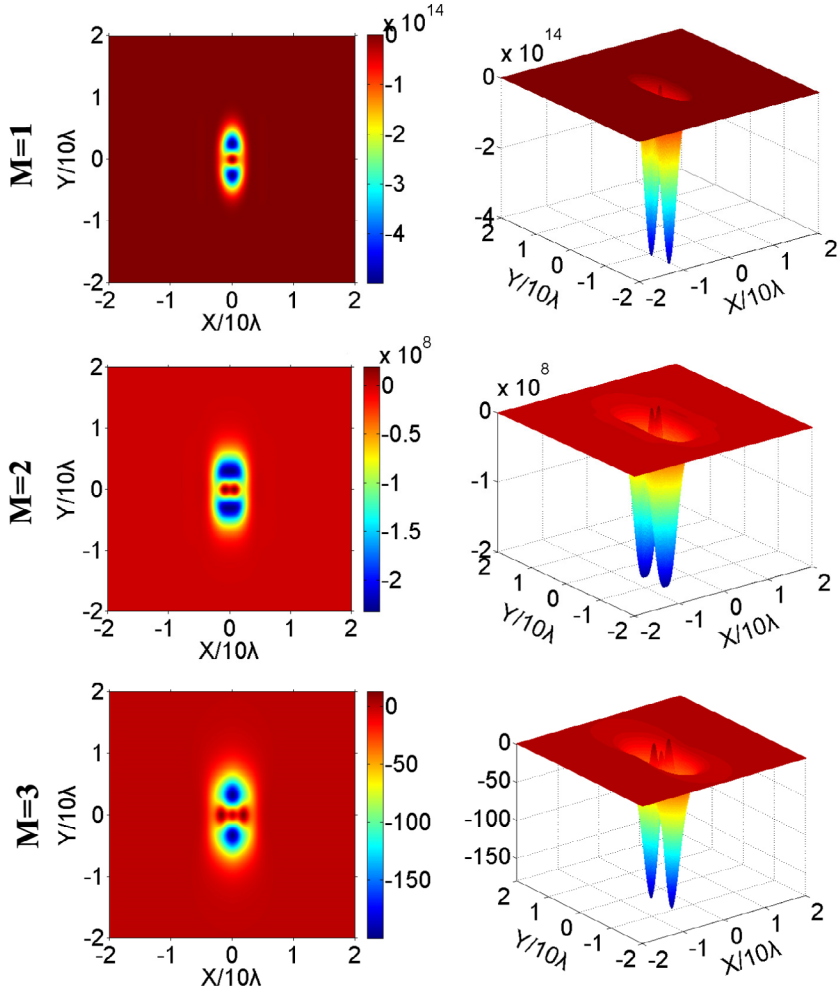

Figure 9. The OAM density distribution of the nonparaxial AHB with OAM of elliptical symmetry in the free space for different TC: $w_{0x} = 0.5\,\lambda$, $w_{0y} = \lambda$, $z = 10z_r$.

propagation distance. Moreover, the phase distributions of the z-component also present lateral dislocation.

From Figure 7, we can see that, with increasing M, in the far field ($z = 20z_r$) the intensity distribution in the x-direction also expands faster than that in the y-direction., So the intensity distribution shows that the longitudinal maximum intensity is gradually shrinking to the centre, and finally becomes a longitudinal maximum. But it still presents a symmetric distribution. As M increases, the phase distributions of the x-component and z-component always present a helicform. The phase distribution of the z-component also has a dislocation.

Figures 8 and 9 show the OAM density distribution of the nonparaxial AHB with OAM with elliptical symmetry for several values of the propagation distance and M, respectively. From Figures 8 and 9, we can see that the OAM density distribution of the nonparaxial AHB with OAM with elliptical symmetry concentrates mostly in two small symmetrical regions, whether in the near field or far field. With increasing propagation distance, the OAM density distribution rotates from the x-direction to the y-direction, and the range of the density distribution is gradually reduced. The OAM density first gradually increases and then decreases. With increasing M, the OAM density distribution gradually expands, and then gradually decreases.

4. Conclusion

Based on the Rayleigh–Sommerfeld integrals formula, analytical expressions for the nonparaxial AHB with OAM in free space are derived. By using these formulae for the electric field components, some numerical examples are given, showing the propagation properties of the nonparaxial AHB with OAM in free space. The normalized intensity distribution and the phase distributions of the nonparaxial AHB with OAM with either circular or elliptical symmetry in free space are studied. The OAM density distributions of the nonparaxial AHB with OAM, having elliptical symmetry in free space, are also demonstrated by numerical examples. We have found that the nonparaxial propagation properties of an AHB with OAM in free space are closely related to the values of, respectively: the beam waists, propagation distances and TC. The patterns of the intensity and the phase distribution of the x-component and z-component can be completely different for certain values of the parameters beam waist, propagation distance and TC. The OAM density distributions of the nonparaxial AHB with elliptical symmetry propagating in free space are also closely related to the propagation distances and TC. Our formulae Equations (11–13) provide a convenient way for studying the nonparaxial and paraxial propagation properties of an AHB with OAM in free space; it also will be useful in the application of the AHB with OAM for optical communication, optical trapping and nonlinear optics, using the wide variety of beam profiles and phases connected with these beams.

Disclosure statement

No potential conflict of interest was reported by the authors.

Funding

This work was supported by the National Natural Science Foundation of China [grant number 11374222]; National Natural Science Fund for Distinguished Young Scholar [grant number 11525418]; the Qing Lan Project of Jiangsu Province; sponsorship of Jiangsu Overseas Research & Training program for University Prominent Young & Middle-aged Teachers and Presidents.

References

(1) Gibson, G.; Courtial, J.; Padgett, M.J.; Vasnetsov, M.; Pas'ko, V.; Barnett, S.M.; Franke-Arnold, S. Free-Space Information Transfer Using Light Beams Carrying Orbital Angular Momentum. *Opt. Express* **2004**, *12*, 5448–5456.

(2) Djordjevic, I.B. Deep-Space and Near-Earth Optical Communications by Coded Orbital Angular Momentum (OAM) Modulation. *Opt. Express* **2011**, *19*, 14277–14289.

(3) Wang, J.; Yang, J.-Y.; Fazal, I.M.; Ahmed, N.; Yan, Y.; Huang, H.; Ren, Y.; Yue, Y.; Dolinar, S.; Tur, M. Terabit Free-Space Data Transmission Employing Orbital Angular Momentum Multiplexing. *Nat. Photonics* **2012**, *6*, 488–496.

(4) Molina-Terriza, G.; Torres, J.P.; Torner, L. Twisted Photons. *Nat. Phys*. **2007**, *3*, 305–310.

(5) Dholakia, K.; Čižmár, T. Shaping the Future of Manipulation. *Phys. Rev. Lett*. **2011**, *5*, 335–342.

(6) Molina-Terriza, G.; Torres, J.P.; Torner, L. Management of the Angular Momentum of Light: Preparation of Photons in Multidimensional Vector States of Angular Momentum. *Phys. Rev. Lett.* **2001**, *88*, 013601.

(7) Gahagan, K.; Swartzlander, G. Optical Vortex Trapping of Particles. *Opt. Lett*. **1996**, *21*, 827–829.

(8) Kitamura, K.; Sakai, K.; Takayama, N.; Nishimoto, M.; Noda, S. Focusing Properties of Vector Vortex Beams Emitted by Photonic – Crystal Lasers. *Opt. Lett*. **2012**, *37*, 2421–2423.

(9) Bekshaev, A.Y.; Sviridova, S.; Popov, A.Y.; Tyurin, A. Generation of Optical Vortex Light Beams by Volume Holograms with Embedded Phase Singularity. *Appl. Phys. Lett*. **2012**, *285*, 4005–4014.

(10) Liu, Y.; Sun, X.; Luo, D.; Raszewski, Z. Generating Electrically Tunable Optical Vortices by a Liquid Crystal Cell with Patterned Electrode. *Appl. Phys. Lett*. **2008**, *92*, 101114.

(11) Liu, Y.; Sun, X.; Wang, Q.; Luo, D. Electrically Switchable Optical Vortex Generated by a Computer-Generated Hologram Recorded in Polymer-Dispersed Liquid Crystals. *Phys. Rev. Lett*. **2007**, *15*, 16645–16650.

(12) Yin, J.; Gao, W.; Zhu, Y. Generation of Dark Hollow Beams and Their Applications. *Prog. Opt*. **2003,** *45*, 119.
(13) Kuga, T.; Torii, Y.; Shiokawa, N.; Hirano, T.; Shimizu, Y.; Sasada, H. Novel Optical Trap of Atoms with a Doughnut Beam. *Phys. Rev. Lett.* **1997**, *78*, 4713.
(14) Vetelino, F.E.S.; Andrews, L.C. In Annular Gaussian Beams in Turbulent Media. *Phys. Rev. Lett*. **2003**, *2003*, 87.
(15) Ito, H.; Nakata, T.; Sakaki, K.; Ohtsu, M.; Lee, K.; Jhe, W. Laser Spectroscopy of Atoms Guided by Evanescent Waves in Micron-Sized Hollow Optical Fibers. *Phys. Rev. Lett*. **1996**, *76*, 4500.
(16) Wang, X.; Littman, M.G. Laser Cavity for Generation of Variable-Radius Rings of Light. *Opt. Lett*. **1993**, *18*, 767–768.
(17) Herman, R.; Wiggins, T. Production and Uses of Diffractionless Beams. *Phys. Rev. A* **1991**, *8*, 932–942.
(18) Lee, H.S.; Stewart, B.; Choi, K.; Fenichel, H. Holographic Nondiverging Hollow Beam. *Phys. Rev. A* **1994**, *49*, 4922.
(19) Marksteiner, S.; Savage, C.; Zoller, P.; Rolston, S. Coherent Atomic Waveguides from Hollow Optical Fibers: Quantized Atomic Motion. *Phys. Rev. A* **1994,** *50*, 2680.
(20) Arlt, J.; Dholakia, K. Generation of High-Order Bessel Beams by Use of an Axicon. *Opt. Commun*. **2000**, *177*, 297–301.
(21) Balykin, V.; Letokhov, V. The Possibility of Deep Laser Focusing of an Atomic Beam into the Å-Region. *Opt. Commun*. **1987**, *64*, 151–156.
(22) Gori, F.; Guattari, G.; Padovani, C. Bessel–Gauss Beams. *Opt. Commun*. **1987**, *64*, 491–495.
(23) Xuan-Hui, L.; Xu-Min, C.; Lei, Z.; Da-Jian, X. High-Order Bessel–Gaussian Beam and Its Propagation Properties. *Chin. Phys. Lett.* **2003**, *20*, 2155.
(24) Cai, Y.; Lu, X.; Lin, Q. Hollow Gaussian Beams and Their Propagation Properties. *Opt. Lett*. **2003**, *28*, 1084–1086.
(25) Cai, Y.; Lin, Q. Hollow Elliptical Gaussian Beam and Its Propagation through Aligned and Misaligned Paraxial Optical Systems. *J. Opt. Soc. Am. A* **2004**, *21*, 1058–1065.
(26) Cai, Y. Model for an Anomalous Hollow Beam and Its Paraxial Propagation. *Opt. Lett*. **2007**, *32*, 3179–3181.
(27) Cai, Y.; Eyyuboğlu, H.T.; Baykal, Y. Propagation Properties of Anomalous Hollow Beams in a Turbulent Atmosphere. *Opt. Commun*. **2008**, *281*, 5291–5297.
(28) Wang, K.; Zhao, C.; Xu, B. Propagation of Anomalous Hollow Beam through a Misaligned First-Order Optical System. *Opt. Laser. Technol*. **2010**, *42*, 1218–1222.
(29) Wang, K.; Zhao, C. Fractional Fourier Transform for an Anomalous Hollow Beam. *J. Opt. Soc. Am. A* **2009**, *26*, 2571–2576.
(30) Wang, K.; Zhao, C. Analytical Solution for an Anomalous Hollow Beam in a Fractional Fourier Transforming Optical System with a Hard Aperture. *Opt. Laser. Technol*. **2012**, *44*, 1232–1239.
(31) Cai, Y.; Wang, F. Partially Coherent Anomalous Hollow Beam and its Paraxial Propagation. *Phys. Lett. A* **2008**, *372*, 4654–4660.
(32) Zhao, C.; Wang, X.; Zhao, C.; Wang, K.; Cai, Y. Statistical Properties of an Anomalous Hollow Beam with Orbital Angular Momentum. *J. Mod. Opt*. **2015**, *62*, 179–185.
(33) Luneburg, R.K.; Herzberger, M., Eds.; *Mathematical Theory of Optics*; University of California Press: California, CA, **1964**.